Astronomical and Astrophysical Transactions (*AApTr*), 2025, Vol. 35, Issue 4, pp. 501–514,
ISSN 1055-6796, Photocopying permitted by license only, ©Cambridge Scientific Publishers

Comparison of radiation fluxes of star-forming regions in the galaxy NGC 1512

E.A. Izmodenova*, K.I. Smirnova

Ural Federal University, 19 Mira Street, Ekaterinburg, 620062, Russia

Received 15 June, 2025; accepted 12 September, 2025

The article presents a comparative study of two catalogs of H II regions Congiu (878 regions) and Groves (626 regions) for the galaxy NGC 1512, selected on the basis of identical observational data from PHANGS-MUSE. The study includes a pixel-by-pixel comparison of data using high-resolution materials obtained with JWST (7.7 μm, 21 μm), ALMA (CO(2-1) line) and MUSE (Hα, Hβ, [OIII]λ5007 lines). It was found that 268 regions from the Congiu catalog are unique. Unique regions are characterized by low flux values in all studied ranges. A characteristic spatial distribution was revealed: regions from the Congiu catalog form a ring-shaped structure around the circumnuclear ring, where regions from the Groves catalog are practically absent. The analysis of the correlations of the considered flows showed an identical dependence between the parameters for both catalogs with minor differences in the values of the correlation coefficients, which remain within the limits of statistical significance. The results demonstrate both consistency and methodological differences in the approaches to identifying H II regions.

Keywords: ISM: H II regions, Galaxies: ISM, Galaxies: photometry, Galaxies: star formation

1 Introduction

Star formation is a key process that determines the evolution of galaxies and the structure of their interstellar medium (ISM). It is characterized by a wide range of manifestations covering various bands of electromagnetic radiation, thus allowing us to study physical properties of interstellar gas and mechanisms of star formation.

Ionized hydrogen regions (H II) associated with young massive OB stars play a significant role in this process. Their intense ultraviolet radiation causes ionization of the surrounding hydrogen, forming bright emission regions that serve as indicators of ongoing star formation. In this study, we analyze the emission of H II regions in the barred spiral galaxy NGC 1512, located in the Horologium constellation at a distance of 18.8 Mpc (Anand et al., 2021). The galaxy has a double ring structure with

*Email: izmodenova2002@gmail.com

active star formation in the central nuclear ring. The interaction with the companion galaxy NGC 1510 causes tidal effects that enhance star formation at the disk periphery (Robin et al., 2024).

Previously, this galaxy was observed in various bands: in the near infrared range (3.3, 6.2, 7.7, 8.6, 11.2, 12.7, 16.4 μm) with the Spitzer and WISE telescopes, in the ultraviolet range with GALEX, and in the far infrared range with Herschel as a part of the KINGFISH project (Kennicutt et al., 2011).

And now our study is based on high-resolution data from the PHANGS-ALMA (CO(2-1) line), PHANGS-MUSE (Hα, Hβ, O III lines) and PHANGS-JWST (7.7 and 21 μm ranges) surveys. Considering that the components of the interstellar medium are not directly observed, but are determined through indirect indicators, several observational ranges are used in this work for a comprehensive study of these components.

Emission in the 7.7 μm range, characteristic of vibrational transitions of polycyclic aromatic hydrocarbons (PAHs) (Murga, 2024), is used to study the star formation rate. PAHs are compounds consisting of benzene rings, and their emission correlates with the star formation rate (Calzetti et al., 2007). Very small grain emission, which is also used to estimate the star formation rate, was observed until recently in the 22 μm (WISE), 24 μm (Spitzer) ranges. Now, with the advent of JWST, it is recorded in the 21 μm range (Belfiore et al., 2023, Chown et al. 2025). In this work, we also use data in this range.

The Hα, Hβ, and O III emission lines indicate the presence of ionized hydrogen. The CO(2-1) spectral line serves as an indicator of molecular hydrogen, which is difficult to observe directly due to its low transparency, while the CO molecule, which consists of oxygen and carbon, is easily excited and detected (Bolatto et al. 2013). Based on the PHANGS-MUSE data, two catalogs of H II regions were created using different extraction methods. The catalog created by Groves et al. (2023) and the catalog created by Congiu et al. (2023). The aim of the study is to analyze the differences in the parameters of the ISM of the selected star forming regions depending on the method used to extract the regions of the two catalogs.

This paper contains the following sections: Section 2 describes the used catalogs of H II regions, Section 3 describes the method for obtaining radiation fluxes and comparing the obtained dependencies, and Section 4 summarizes the results of our study.

2 Used catalogs

This study utilizes two nebula catalogs based on PHANGS-MUSE data and Hα line maps, compiled by different research teams. In both catalogs, NGC 1512 is part of a sample of 19 nearby spiral galaxies.

The first catalog, presented in Groves et al. (2023), was obtained using the HIIphot method[1] (Kreckel et al. 2019), specifically designed to identify H II regions based on Hα maps. The region boundaries are determined by the peaks of Hα emission and

[1]https://web.archive.org/web/20161204020654/http://dolomiti.pha.jhu.edu/dthilker/HIIphot_code/

then expanded through iterative Gaussian smoothing. This catalog includes a total of 30790 identified regions across all 19 galaxies.

The second catalog, proposed by Congiu et al. (2023), was compiled using the CLUMPFIND algorithm[2] (Williams et al. 1994). This algorithm employs a contour-based approach, initially detecting local emission peaks and subsequently assigning surrounding pixels within the same contour to the nearest peak. This method allows for the identification of different types of nebulae (H II regions, planetary nebulae, and supernova remnants) based on a composite image created from integrated flux maps of the Hα, [OIII]λ5007 and the [SII]$\lambda\lambda$6717, 6731 doublet lines. The final catalog identifies 40920 nebulae across all sample galaxies, of which 29986 (73%) are classified as H II regions.

Given the differences in catalog construction methods, a comparative analysis of star-forming region maps in NGC 1512 is of interest.

It is important to note that Congiu et al. (2023) presented a comparative study of their new catalog with the previously published catalog by Groves et al. (cited as Santoro et al., 2022). The analysis revealed significant differences in source identification: the Congiu catalog provides broader coverage, detecting a larger number of regions with substantially greater spatial extent compared to the results of the Groves catalog.

Overlaying the two nebula maps (Figure 1) reveals that the Congiu catalog contains a greater number of identified regions: 878 nebulae are classified as H II regions, whereas the Groves catalog includes 626 H II regions.

Figure 1 presents an intriguing distribution of identified nebulae: in the central region of the galaxy, nebulae from both catalogs overlap, forming a nuclear ring with a nebula at its core. Beyond this, there is a zone almost devoid of regions from the Groves catalog, followed by another ring of overlapping regions.

The observed structure of nebular distribution in NGC 1512 reveals systematic differences in the region identification methods used in the two catalogs. The noticeable gap in the distribution of regions in the Groves catalog suggests potential limitations in the methodology employed by Groves for identifying regions in this area.

The pixel-by-pixel comparison of the data within the H II regions revealed significant differences between the catalogs. 268 regions from the Congiu catalog have no matches in the Groves catalog, which confirms their uniqueness. The assessment of the integral fluxes in unique regions in all spectral ranges demonstrates low values, which is consistent with the previously established characteristics of the Congiu catalog (Congiu et al., 2023), which is distinguished by the predominance of low-intensity regions. At the same time, 604 regions of the Congiu catalog demonstrate partial spatial overlap with objects in the Groves catalog, while 6 regions completely coincide with the regions identified in the Groves catalog.

Ultimately, we have two catalogs compiled by different research teams, where the same data has been used to identify distinct sets of regions.

[2]https://home.ifa.hawaii.edu/users/jpw/clumpfind.shtml

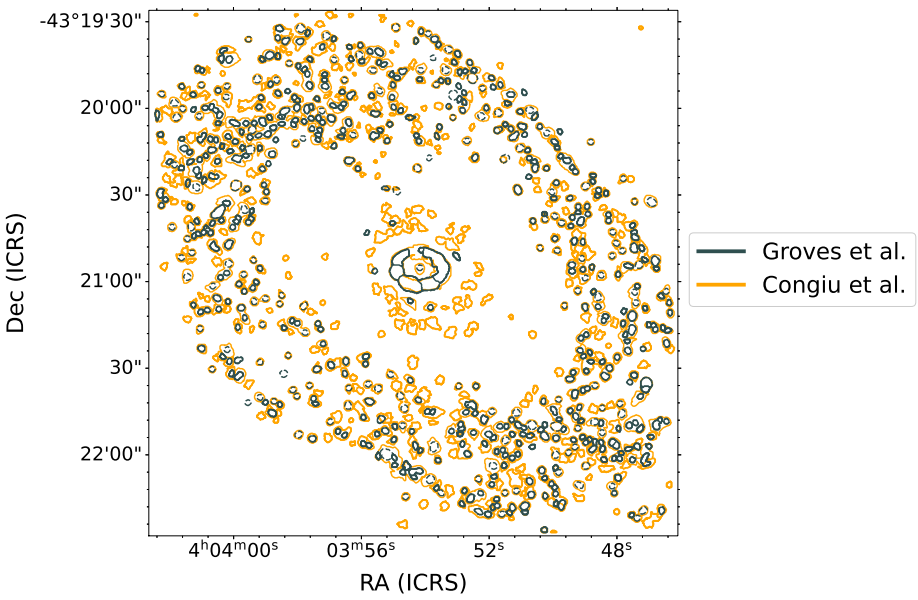


Figure 1 Overlay of nebula maps. Regions identified by Groves et al. are highlighted in gray, while regions identified by Congiu et al. are highlighted in orange.)

3 Comparison of radiation fluxes

3.1 Methodology

This study utilizes high-resolution data, including JWST (7.7 μm, 21 μm) (Lee et al. 2023), ALMA (CO(2-1) line) (Leroy et al. 2021), and ALMA-MUSE (Hα, Hβ, [OIII]λ5007 lines) (Emsellem et al. 2022).

In the studied spectral ranges, different types of emission serve as indicators of interstellar medium (ISM) components involved in star formation (SF). The CO(2-1) line characterizes cold diffuse gas. while the emission lines Hα, Hβ, [OIII]λ5007 indicate the presence of ionized hydrogen. Infrared emission at 7.7 μm serves as a marker of polycyclic aromatic hydrocarbons (PAHs), whereas emission at 21 μm is an indicator of dust grains.

It is important to note that PAHs and dust grains have different spatial distributions (Topchieva et al. 2017), making it interesting to analyze them separately.

The pixels of all FITS files were resampled to a uniform size using the script, which aligns images to a reference file. A mask file for each catalog was used as the reference. Since all data had comparable resolution, no additional normalization was required.

Radiation flux measurements were carried out using the aperture photometry method.

To assess the relationship between the data sets, the Spearman correlation coefficient (ρ) was calculated using the SciPy library module "scipy.stats"[3]. This correla-

[3]https://docs.scipy.org/doc/scipy/reference/stats.html

tion coefficient was chosen because it is applicable to non-normally distributed data, is robust to outliers, and describes not only linear but any monotonic relationship (Cohen, 2023). It has also been previously employed in the works of Smirnova et al. (2017, 2019). Additionally, the number of regions involved in each comparison is provided. The final Spearman coefficient values and the number of regions are presented in the graphs for both catalogs.

3.2 Analysis of the comparison graphs

A variety of graphs illustrating the comparisons of emission fluxes have been obtained. These relationships will be examined in detail in the following sections.

The comparison of fluxes between 7.7 and 21 μm was shown in Figure 1 of Izmodenova and Smirnova (2025). The observed correlation for SF regions from both catalogs between fluxes in the near- and mid-infrared ranges indicates that both components are activated (excited) by the same radiation source.

As mentioned earlier, PAHs and fine dust exhibit different spatial distributions: PAHs are destroyed by UV radiation and therefore are located farther from UV sources compared to fine dust. Consequently, at small scales, the emission peaks in the 7.7 μm and 21 μm ranges will be spatially offset from each other. In addition, PAH emission is strongly dependent on metallicity. For this reason, the correlation between the 7.7 μm and 21 μm emissions decreases (Chown et al. 2025; Whitcomb et al. 2023; Villanueva et al. 2025). This mismatch between the 7.7 μm and 21 μm emissions results in scatter in the data points on the plot.

Considering the characteristics of region identification in both catalogs, particular interest was given to studying the relationship between emission fluxes and the flux in the Hα line, which serves as an indicator of ionized hydrogen. It is important to note that the Hα fluxes were refined relative to those presented in Izmodenova and Smirnova (2025). By analyzing the correlation between fluxes in Figures 2a,b, 3a,b, it can be inferred that the evolution of PAHs and small dust grains is closely linked to UV radiation in the vicinity of ionized hydrogen regions.

In these Figures, as well as in all subsequent ones, data points obtained using the Groves et al. catalog are shown in gray, while those from the Congiu et al. catalog are displayed in orange. The Spearman correlation coefficient (ρ) and the number of data points (n) are indicated in the legend in the upper left corner.

A similar conclusion regarding the influence of UV radiation on the evolution of PAHs and dust grains can be drawn by analyzing the correlations between fluxes in the 7.7 μm and 21 μm ranges and the fluxes in the O III line in Figure 4a,b.

The comparison of molecular (CO line emission) and ionized (Hα, Hβ lines) hydrogen indicators, presented in Figure 5a,b, demonstrates a correlation between the parameters. This may result from both states being present within the identified region.

The flux correlation graphs for the CO line and infrared bands at 7.7 μm and 21 μm (Figures 6a,b) confirm the presence of PAHs and small dust grains in molecular hydrogen regions.

By analyzing the flux correlation graphs for the O III line and the Hα, Hβ lines, presented in Figure 7a,b, it can be concluded that gas ionization is primarily driven by young OB stars. This is particularly evident in Figure 7b, where the Spearman correlation coefficient $\rho = 0.89$ for both catalogs.

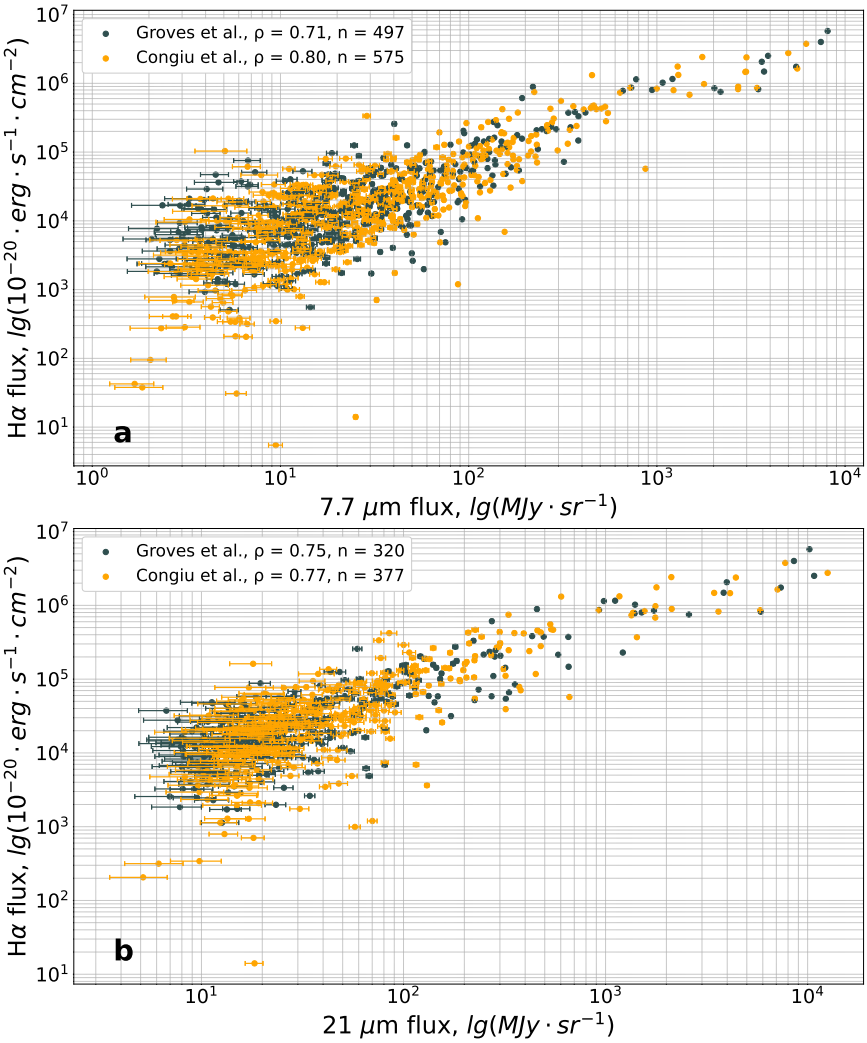


Figure 2 Correlation plot of 7.7 μm flux and Hα line (a); correlation plot of 21 μm flux and Hα line (b). Data points obtained using the Groves et al. catalog are shown in gray, while data points from the Congiu et al. catalog are shown in orange. The Spearman correlation coefficients and the number of data points are indicated in the legend in the upper left corner.

The correlation between the fluxes in the Hα and Hβ lines, presented in Figure 8, is expected, as both lines are hydrogen recombination lines that originate in the same H II regions.

All presented graphs demonstrate a positive correlation between the investigated emission fluxes. Despite differences in nebula identification methods across the catalogs, the data points from both catalogs exhibit a similar distribution within each correlation plot.

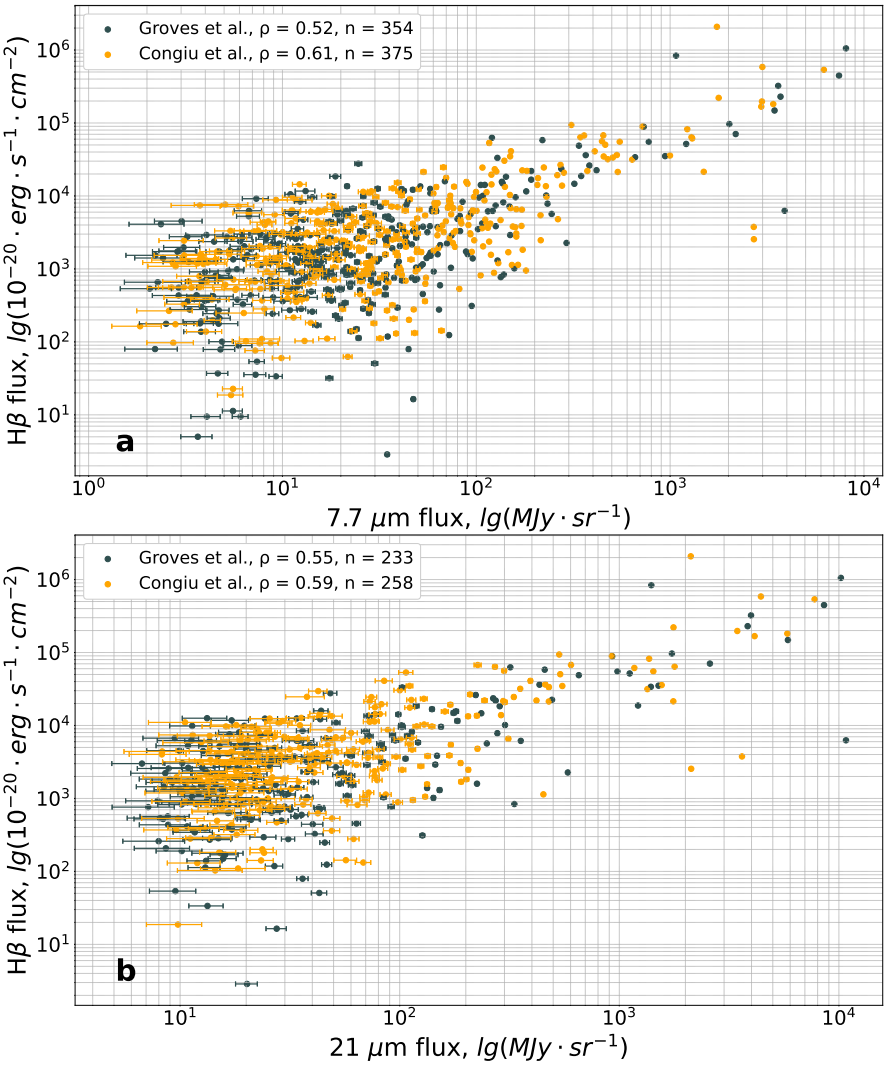


Figure 3 Correlation plot of 7.7 μm flux and Hβ line (a); correlation plot of 21 μm flux and Hβ line (b). Data points obtained using the Groves et al. catalog are shown in gray, while data points from the Congiu et al. catalog are shown in orange. The Spearman correlation coefficients and the number of data points are indicated in the legend in the upper left corner.

It should also be noted that in the low-flux regions of Figures 2, 4a, 5a, 7a, 8, the data points are predominantly those identified using the Congiu catalog. This likely reflects the fact that multiple emission-line maps were employed in constructing the catalog, allowing fainter sources to be detected.

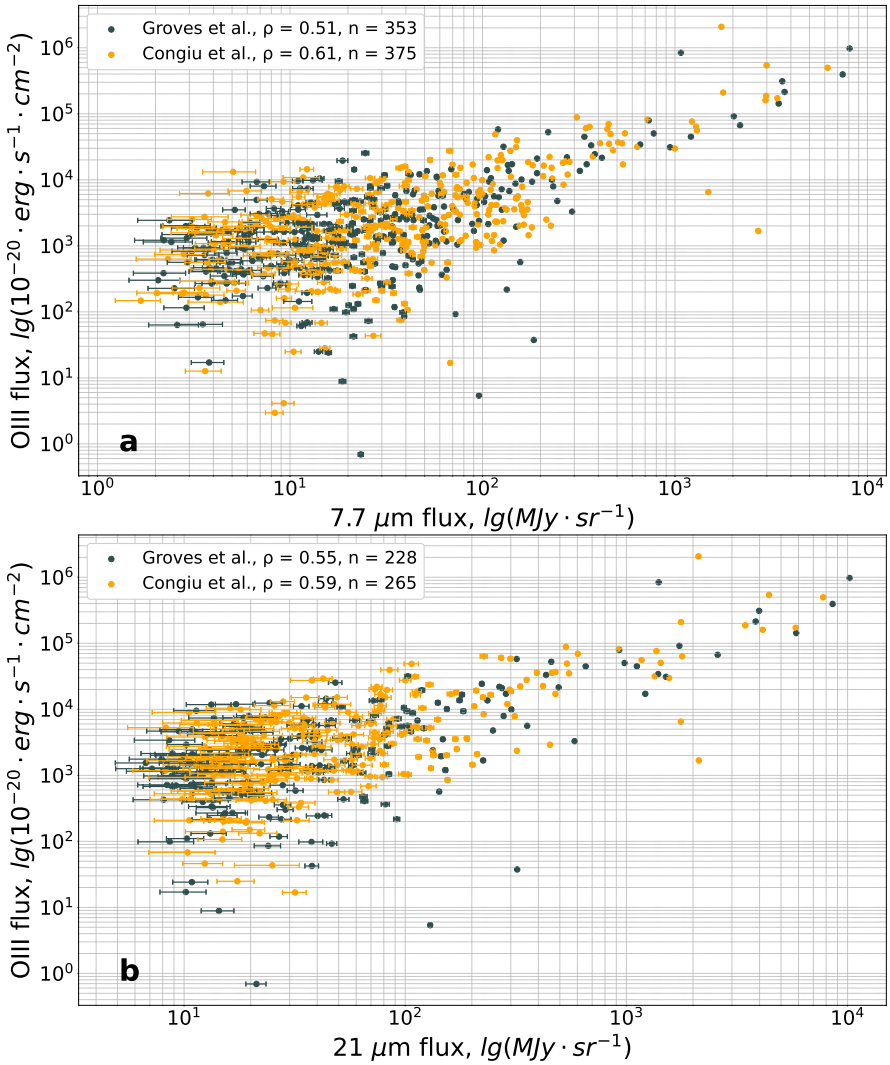


Figure 4 Correlation plot of 7.7 μm flux and O III line (a); correlation plot of 21 μm flux and O III line (b). Data points obtained using the Groves et al. catalog are shown in gray, while data points from the Congiu et al. catalog are shown in orange. The Spearman correlation coefficients and the number of data points are indicated in the legend in the upper left corner.

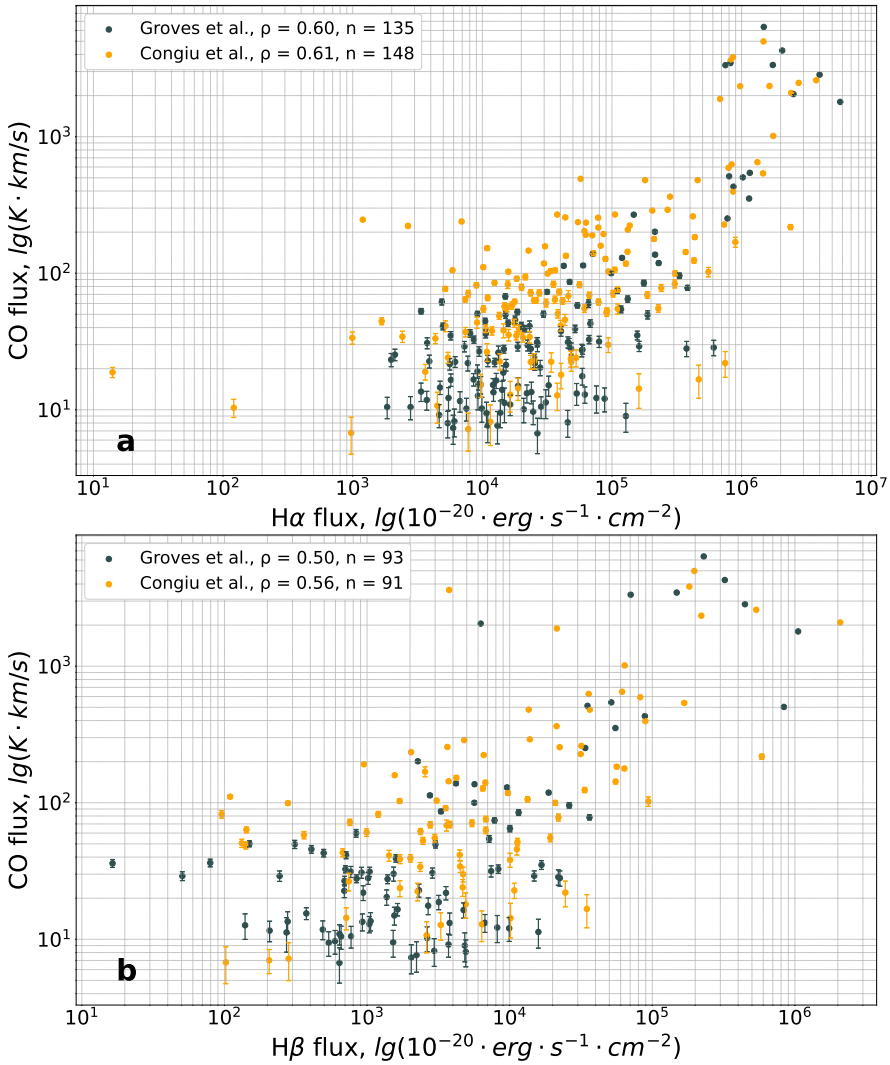


Figure 5 Correlation plot of Hα flux and CO line flux (a); correlation plot of Hβ flux and CO line flux (b). Data points obtained using the Groves et al. catalog are shown in gray, while data points from the Congiu et al. catalog are shown in orange. The Spearman correlation coefficients and the number of data points are indicated in the legend in the upper left corner.

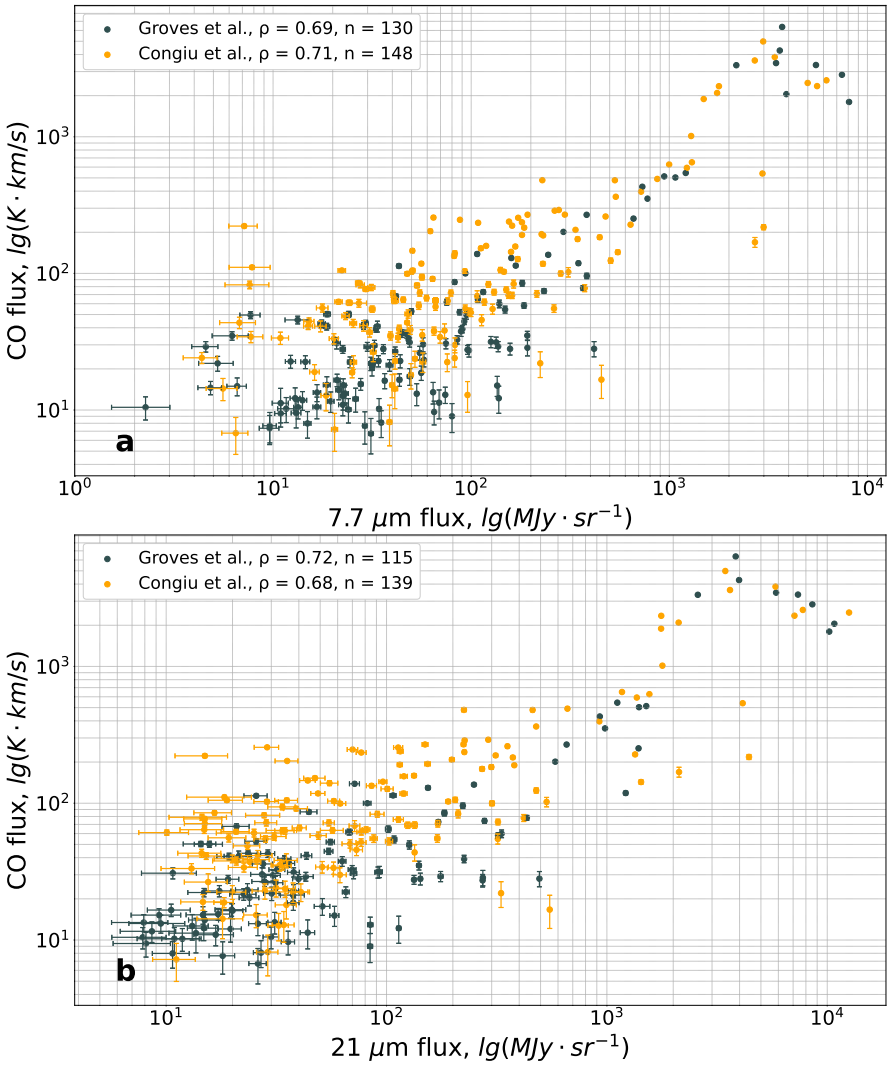


Figure 6 Correlation plot of 7.7 μm flux and CO line flux (a); correlation plot of 21 μm flux and CO line flux (b). Data points obtained using the Groves et al. catalog are shown in gray, while data points from the Congiu et al. catalog are shown in orange. The Spearman correlation coefficients and the number of data points are indicated in the legend in the upper left corner.

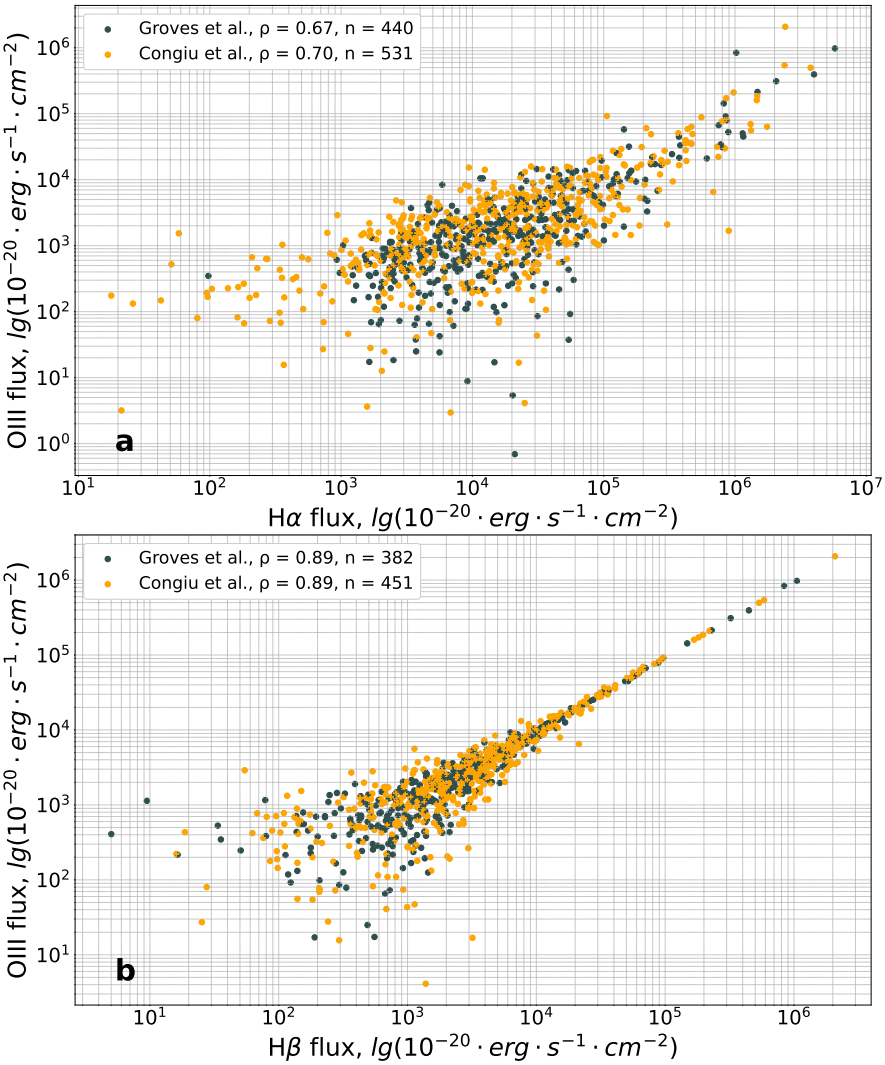


Figure 7 Correlation plot of Hα flux and O III line (a); correlation plot of Hβ flux and O III line (b). Data points obtained using the Groves et al. catalog are shown in gray, while data points from the Congiu et al. catalog are shown in orange. The Spearman correlation coefficients and the number of data points are indicated in the legend in the upper left corner.

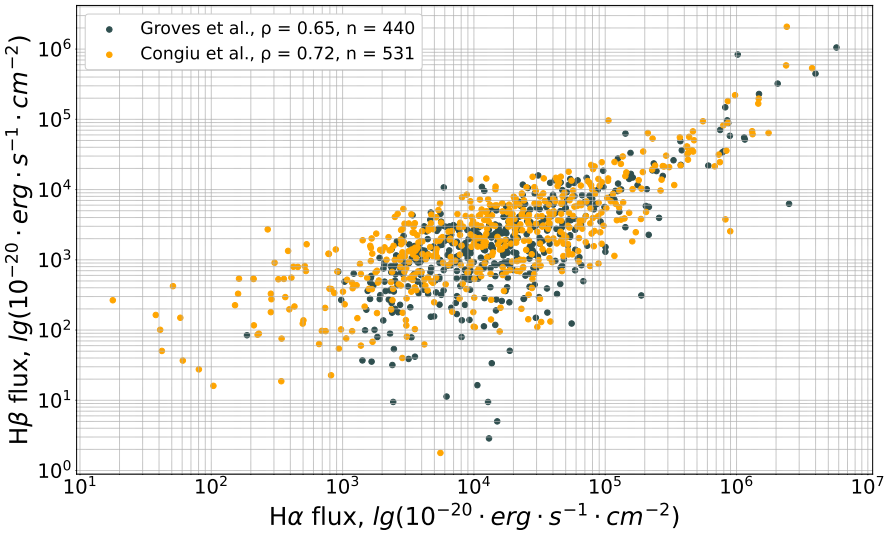


Figure 8 Correlation plot of Hα and Hβ lines. Data points obtained using the Groves et al. catalog are shown in gray, while data points from the Congiu et al. catalog are shown in orange. The Spearman correlation coefficients and the number of data points are indicated in the legend in the upper left corner.

4 Conclusions

This study compared the characteristics of the H II regions of two independent catalogs (Congiu et al. and Groves et al.), constructed on identical observational data of the galaxy NGC 1512. The analysis demonstrates the consistency of the results in most cases, although there are certain discrepancies.

1. The Congiu catalog identifies a significantly larger number of H II regions in NGC 1512. Spatial analysis reveals a characteristic distribution: regions from the Congiu catalog form a ring-like structure around the circumnuclear ring, where regions from the Groves catalog are nearly absent. These unique regions are characterized by low flux values across all studied ranges, which is attributable to differences in the methodologies used for region extraction.
2. The correlation analysis of fluxes revealed identical dependencies between parameters for both catalogs, with the data points lying along a common trend line, albeit in different coordinate regions. The correlation coefficient values show only minor discrepancies between the catalogs, yet all of them meet the criteria of statistical significance.

Acknowledgements

The authors sincerely thank the anonymous reviewers for their critical comments and constructive suggestions, which contributed to a significant improvement of both the content and the presentation of this paper.

K. Smirnova has been supported by the Ministry of Science and Education of Russia, the FEUZ-2025-0003 project.

This work made use of Astropy, a community-developed core Python package and an ecosystem of tools and resources for astronomy (Astropy Collaboration et al., 2013, 2018, 2022), APLpy, an open-source plotting package for Python (Robitaille and Bressert, 2012; Robitaille, 2019), NumPy (Harris et al., 2020), Matplotlib (Hunter, 2007).

References

Anand G. S. et al. (2021) MNRAS 501, 3621
Astropy Collaboration et al. (2013) AAp 558, A33
Astropy Collaboration et al. (2018) AJ 156, 123
Astropy Collaboration et al. (2022) ApJ 935, 167
Belfiore F. et al. (2023) AAp 678, A129
Bolatto A. D., Wolfire, M., Leroy, A. K. (2013) ARAA 51, 207
Calzetti D. et al. (2007) ApJ 666, 870
Chown R. et al. (2025) ApJ 987, 91
Cohen M. X. (2023) Modern Statistic: Intuition, Math, Python, R, p. 468
Congiu E. et al. (2023) A&A 672, A148
Emsellem E. et al. (2022) A&A 659, A191
Groves B. et al. (2023) MNRAS 520, 4902
Hunter J. D. (2007) Computing in Science & Engineering, 9, 90
Harris R. C. et al. (2020) Nature 585, 357
Izmodenova E. A., Smirnova K. I (2025) Physics of Space: Proceedings of the 52nd All-Russian Student Scientific Conference with International Participation 2025, 299
Kennicutt R. C. et al. (2011), PASP 123, 1347
Koribalski B. S. et al. (2004) AJ 128, 16
Kreckel K. et al. (2019) ApJ 887, 80
Lee J. C. et al. (2023) ApJL 944, L17
Leroy A. K. et al. (2021) ApJS 255, 19
Murga M. S. (2024) Phys. Usp. 67, 961
Robin T. et al. (2024) A&A 681, A7
Robitaille T., Bressert E. (2012) APLpy: Astronomical Plotting Library in Python, Astrophysics Source Code Library
Robitaille T. (2019) APLpy v2.0: The Astronomical Plotting Library in Python
Santoro et al. (2022) A&A 658, A188
Smirnova K. I., Wiebe D. S. (2019) ARep 63, 445
Smirnova K. I., Wiebe D. S., Moiseev A. V. (2017) Open Astronomy 26, 88

Topchieva A. P., Wiebe D. S., Kirsanova, M. S., Krushinskii V. V. (2017) ARep 61, 1015
Villanueva V. et al. (2025) AAp 695, A202
Whitcomb C. M., Sandstrom K., Leroy, A., Smith J. -D. T. (2023) ApJ 948, 88
Williams J. P., de Geus E. J., Blitz L. (1994) ApJ 428, 693